Available online at www.sciencedirect.com
SCIENCE DIRECT®
Computer Networks 47 (2005) 751–763
Computer Networks
www.elsevier.com/locate/comnet

Radio frequency channel modeling for proximity networks on the Martian surface

Vishwanath Chukkala, Phillip DeLeon *, Stephen Horan, Vijayakumar Velusamy

Klipsch School of Electrical and Computer Engineering, Center for Space Telemetering and Telecommunications, New Mexico State University, Box 30001, Dept. 3-0, Las Cruces, NM 88003, USA

Available online 2 October 2004

Abstract

NASA's long-term goals for the exploration of Mars include the use of rovers and sensors which communicate through proximity wireless networks. The performance of any such wireless network depends fundamentally on the radio frequency (RF) environment. In order to evaluate and optimize the performance of such a wireless network, a basic understanding or model of the channel is important. In this paper, we present our results concerning the RF environment at selected sites on the surface of Mars with a focus on the link budget and RF coverage patterns. These results take into account the local topography using data from the Mars Global Surveyor, surface reflections, clutter, atmospheric absorption, etc., and contribute to a more accurate RF channel model. We consider a basic wireless network model and demonstrate the possibility for good site coverage and long links despite low antenna heights and radiated power. With such a channel model, mission operators can update elements of the wireless network after deployment with more accurate RF propagation information. Such updates could be used to extend the reach of the network or protect network elements from communication outages due to unforeseen features of the local topography.

Keywords: Mars communications; Wireless proximity networks; RF propagation modeling

1. Introduction

NASA's long-term goals for the exploration of Mars include the use of rovers and sensors which communicate through proximity wireless networks. Elements of the network have a short transmission range, low power requirements, low cost, and a relatively short life span [1]. The performance of any such wireless network depends *fundamentally* on the radio frequency (RF) environment. In order to evaluate and optimize the performance of such a wireless network, a basic understanding or model of the channel is important. With such a model, better choices for the modulation and coding schemes, equalizer design,

* Corresponding author.
E-mail address: pdeleon@nmsu.edu (P. DeLeon).

1389-1286/$ - see front matter
doi:10.1016/j.comnet.2004.08.011

and positioning of access point antennas can be made [2]. These choices can also affect the overall design and operations of a rover or a sensor web for a planetary environment.

Previous missions to Mars which included robotic exploration operated in the UHF frequency band over short ranges and at relatively low data rates [3,4]. For example, the Sojourner rover from the 1997 Mars Pathfinder mission, used a 9600 bps link designed for a maximum extent of 500 m [4]. The Spirit and Opportunity rovers from the 2004 Mars Exploration Rover (MER) mission also used UHF links. Future missions, involving more complex wireless networks will evolve to higher frequency links in S-Band or X-Band in order to support data transfer rates exceeding 1 Mbps [3].

In this research regarding RF channel modeling on the Martian surface, we assume a proximity network model composed of multiple surface rovers and sensors that communicate to a network access point placed on the lander. At the lander, data is filtered, aggregated, and packaged for transmission back to Earth via an orbiting relay station [5]. Other assumptions in the network model are 1 W transmitter power between the access point and surface nodes (rovers or sensors), omni directional antennas placed at a 1 m height, and 2.4 GHz (S-band) carrier frequency. Note, these parameters can be easily changed to meet specific mission configurations. Consideration of this carrier frequency allows evaluation for potential use of off-the-shelf WiFi components (with appropriate modifications for space use). The two main communications issues with respect to evaluation of a channel under the above scenarios are link budget and time dispersion. The link budget is determined by the propagation path loss or the average amount of received power (relative to transmitted power) at a particular distance or location from the transmitter. Time dispersion arises due to multipath propagation whereby replicas of the transmitted signal reach the receiver with different delays due to reflections and scattering.

In order to *accurately* simulate RF coverage patterns and power delay profiles (received power due to multipath as a function of time) at particular sites on the surface of Mars, several effects should be taken into account. These effects include not only the normal $1/R^2$ space loss but also atmospheric absorption (using the atmospheric chemical composition), and surface reflections (using site-specific, soil composition data). In addition, there may be effects due to the local environment such as those from nearby topographic features and surface clutter (rocks). Finally, Mars' planetary curvature must be taken into account for accurately modeling line-of-sight (LOS) distances. With the RF model partially based on the local environment, mission operators can update elements of the wireless network after deployment with more accurate RF propagation information. This information would be developed through Earth-based simulation of RF coverage once visual surface information and location of the lander is obtained. Such updates could be used to extend the reach of the network or protect network elements from communication outages due to unforeseen features of the local topography.

In this paper, we present our results concerning the RF environment at selected sites on the surface of Mars with a focus on the link budget and RF coverage patterns. These results contribute to a model for effectively deploying wireless proximity networks which are expected to be important for rover operations and ground-level sensor networks on the Martian surface. The techniques developed here are also applicable in other communications scenarios with appropriate modifications. This paper is organized as follows. In Section 2, we describe the simulation software, propagation model, and the simulation variables specific to RF propagation on the Mars surface. In Section 3, we describe the sites on Mars selected for this study, associated Digital Elevation Maps (DEMs), and synthesis of a clutter layer for evaluating the impact on propagation due to rocks. In Section 4, we present specific information regarding the assumed network model as well as metrics used in evaluating the results. We present and analyze results including antenna coverage patterns and received signal power, and quantify the impact of surface clutter. Finally, we consider some example applications and present data on area coverage as a function of distance from the network access point. The example applications could be useful

to mission planners and operators and further illustrate the utility of the channel modeling.

2. Simulation software

In planning cellular telephone networks, the industry draws on a number of RF modeling, propagation, and planning tools. These powerful computational tools allow system planners to optimally place cellular base stations by simulating the RF coverage patterns and multipath, among other things. These simulations are based on well-known propagation models and utilize site-specific topographic information as well as locations of man-made structures. Verification of simulation results is typically made with independent field measurements. Although obviously designed for modeling terrestrial systems, with appropriate modifications these tools have the potential to also model RF propagation associated with proximity wireless networks on the Martian surface. For this work, which focusses on modeling the RF coverage patterns for the network scenario described above, we use ATDI's HertzMapper RF propagation software [6]. Next, we describe required modifications to the software and propagation model for use in the Martian environment.

2.1. Propagation model

We have selected the option of using the Irregular Terrain Model (ITM, also known as the Longley-Rice model) as the propagation model in the software simulations [7]. The ITM is a general-purpose propagation model for frequencies between 20 MHz and 20 GHz that predicts the median attenuation of an RF signal as a function of distance and the variability of the signal in time and space based on electromagnetic theory and statistical analysis of terrain. In addition to taking into account the terrain (which is the major factor in propagation modeling on Mars), other reasons for this choice are as follows. First, the ITM is semi-deterministic compared with other models which are empirical. Second, the ITM takes into account atmospheric conditions while other models such as Bullington or Okumura do not. Third, the ITM uses reflection, diffraction, and scattering techniques to calculate the attenuation, while other models may only use one of these effects.

2.2. Simulation variables

Table 1 identifies the key parameters used in the ITM [7]. Of these, only code defining the environmental parameters in the ITM needs modification for simulation of the Mars environment. The first modification is for the electrical ground constants for Mars estimated from soil composition to be as follows: permittivity is 4.0 and conductivity is 10^{-8} S/m [8].

Next, modifications for attenuation due to atmospheric effects are accounted for as follows. First, the surface pressure on Mars is approximately 6.1 mbars which is about 1/150th of the average pressure on Earth [9]. Second, the Martian troposphere consists of almost entirely of dry air and the atmospheric water content near the surface is at least 3000× lower than on Earth [10]. Third, the major constituents of the Martian atmosphere are given in Table 2 [10]. As can be seen, the Martian atmosphere is dominated by carbon dioxide and nitrogen gases. The physical properties of these components reveal that they do not have electric or magnetic dipoles and so

Table 1
Parameters used in the irregular terrain model

Group	Parameter	Values
System	Frequency	2.4 GHz
	Distance	1–30 km
	Antenna height	1 m
	Antenna polarization	Vertical
Environment	Terrain irregularity	Calculated from DEM
	Electrical ground constant	
	Permittivity	4.0
	Conductivity	1.0^{-8} S/m
	Surface refractivity	Chosen so that effective radius, $k = 1$
	Radio climate	Vacuum
Mode		Point-to-point
Statistics	Situation variability	35%

Table 2
Composition of the Mars atmosphere

Carbon dioxide	95.32%
Nitrogen	2.7%
Argon	1.6%
Oxygen	0.13%
Carbon monoxide	0.08%

do not absorb electromagnetic energy. Fourth, although, atmospheric particulates, such as dust or CO_2 ice might cause some attenuation, we do not believe that particulates that are light enough to be suspended in such a diffuse atmosphere could do much radio attenuation, unless they are highly electrically conductive [11]. Actual calculations of the attenuation due to the atmosphere for a horizontal path on Mars' surface, yields approximately 10^{-6} dB/km at 2.5 GHz [10]. Thus, we consider atmospheric attenuation on Mars to be negligible. Similar conclusions can be found in [5].

Modifications for atmospheric refraction are as follows. Given the fact that Mars' atmosphere is so diffuse, even at the planet's surface, it is for practical purposes, a vacuum compared to the Earth's. Thus we assume that any effects due to atmospheric refraction are also negligible in our study [10,11]. The attenuation due to refraction from Earth's atmosphere is normally taken into account by introducing an "effective radius" multiplier. In typical propagation software codes, this multiplier, K is set to 1.33 for all conditions, i.e., the effective radius for Earth is $K \times r_e$ where r_e is the Earth's radius. Since the attenuation due to refraction for Mars is negligible, we set $K = 1$ and use the actual radius of Mars, r_m. Thus for refraction calculations, Mars' effective radius is equal to its actual physical radius. We note that in some software codes, an effective curvature (inverse of the effective radius) is used.

Finally, the ITM code computes the *terrain irregularity* values directly from the DEM data. In addition, the value chosen for *situation variability* is based on matching simulation data to actual field measurements of received RF power using the assumed network model. Simulations and field measurements were made at remote areas in southern New Mexico which were free of man-made objects and vegetation and topographically similar to the Gusev datasets.

3. Digital elevation maps for Mars

3.1. Description of DEMs

In order to develop the planetary RF channel model and, in particular, the RF coverage patterns, a high-resolution DEM must be available for the sites of interest. The largest collection of planet-wide data for Mars is from the Mars Orbiter Laser Altimeter (MOLA) which was part of the 1999 Mars Global Surveyor mission [12]. However, this data set has a maximum spatial resolution of 128 pixel/degree or approximately 400 m/pixel. While this is good enough for general visualization of the region, it is too coarse for modeling terrain on the order of a 1000 m baseline. To examine the effects of RF propagation where the wavelength is on the order of 0.125 m (2.4 GHz), one might expect that a DEM with similar-order resolution is required. However, for typical planning of cellular systems, DEMs with a 1–10 m/pixel resolution are sufficient and successfully used in industry.

To assist in planning the 2004 MER missions, high-resolution maps of four candidate landing areas were developed by the United States Geological Survey (USGS) [13,14]. These datasets are limited to small areas since they are based on available image pairs from the Mars Orbiter Camera-Narrow Angle (MOC-NA). These pairs are used to generate a stereoscopic image and are then processed and tied to MOLA reference elevations [15]. For this study, the USGS Gusev1 and Gusev3 datasets (see Fig. 1) are used in the RF channel modeling due to the range of topographic features they encapsulate within the predicted MER landing ellipse. The datasets have a resolution of 0.000171 degrees/pixel or 10.4 m/pixel at the surface of Mars and are subsampled to 11 m/pixel for compatibility with the software. The subsampling does not have any significant effect on the accuracy due to the small areas under study. The DEMs do not include a physical warping function normally used to compensate for deviations from a

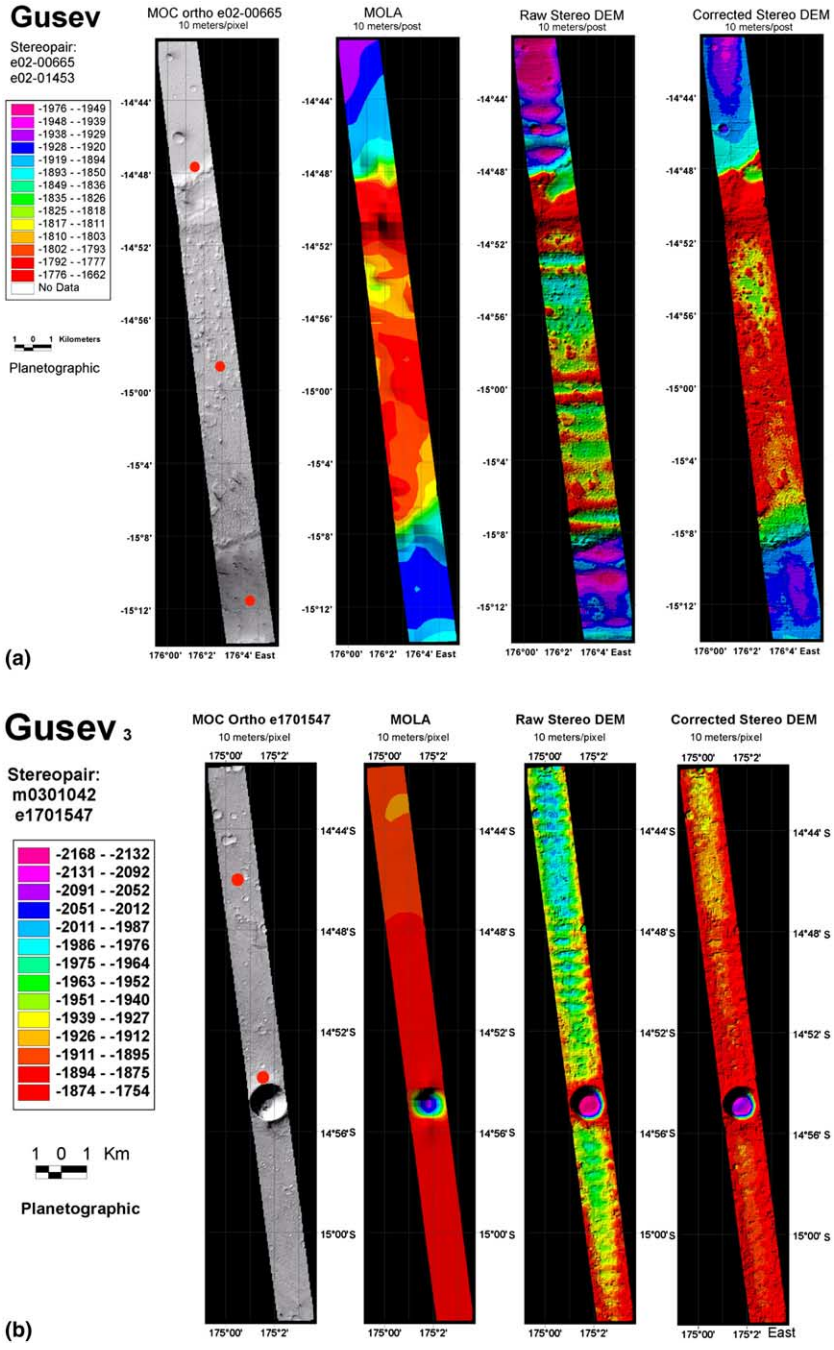

Fig. 1. (a) Gusev1 and (b) Gusev3 datasets, covering areas inside the 2004 MER Gusev Crater landing ellipse. Red discs in left-most picture indicate approximate sites for simulated network access points. The top-most disc of each dataset is "Site 1," the next disc is "Site 2", etc. (For interpretation of the references in colour in this figure legend, the reader is referred to the web version of this article.)

Table 3
Sites for RF simulations

Site	Mars latitude	Mars longitude	Elevation (m)
Gusev1, Site 1	14°47′39.35″S	176°1′29.18″E	83
Gusev1, Site 2	14°58′41.95″S	176°2′53.51″E	158
Gusev1, Site 3	15°11′35.66″S	176°4′31.23″E	24
Gusev3, Site 1	14°53′58.64″S	175°1′28.55″E	264
Gusev3, Site 2	14°45′59.43″S	175°0′28.32″E	182

perfect sphere. However, for the small areas under study, such a warping function is not required.

3.2. Description of simulation sites

The Gusev1 dataset has three sites within the DEM that appear to be candidates for different RF effects. The first site [top red disc in Fig. 1(a)] is at a boundary between what appears to be a flat crater basin and the crater wall. The second site [middle red disc in Fig. 1(a)] is in a region that appears to have significant washout of rocks and rubble. The third site [bottom red disc in Fig. 1(a)] appears to be another crater basin but one that is not as smooth as the first. The Gusev3 dataset has two sites of interest for investigation. The first [top red disc in Fig. 1(b)] appears to be a field with a number of small craters. The second site [bottom red disc in Fig. 1(b)] is close to a relatively large crater with a sharp wall. The coordinates for the five sites used in the RF modeling are given in Table 3.

3.3. Synthesis of clutter layer

Due to the assumption of a 1 m antenna height at the base station, we also consider the effects of surface clutter from rocks on the RF coverage. Since the DEMs used in simulations have an 11 m/pixel resolution, any features below 11 m in size (such as meter-size rocks) will not be revealed. Fortunately, statistics on the rock size and spacing at other sites, based on images from the Viking (1976) and Pathfinder (1997) missions, have been published [16]. Using the statistical distributions for rock size and spacing but applied to the Gusev sites, we create a *synthetic* clutter layer at a resolution of 1 m/pixel and combine it with the upsampled 1 m/pixel DEM. In order to keep the computation reasonable at such fine resolutions, we only consider a 2 km × 2 km area centered on Gusev1, Site 1 [see Fig. 1(a)]. Since the simulation software is not capable of sub-meter resolution due to the inherently large computation involved, rock diameters must be quantized to integer values, e.g., 1 m diameter, 2 m diameter, etc., The quantization boundary levels are chosen to closely match the quantized rock diameters to the statistical distributions and are given in Table 4. Note that at the Pathfinder landing site, the cumulative area covered by rocks greater than 1 m diameter is less than 1% [16]. A sample 100 m × 100 m synthetic clutter layer is given in Fig. 2.

Table 4
Quantization rule for mapping rock diameters to integer values

Actual rock diameter, D (m)	Percentage of rocks with diameter, D (%)	Quantized rock diameter, $\widehat{D}$ (m)
$0 < D \leqslant 0.7$	96.5	$\widehat{D} = 0.0$
$0.7 < D \leqslant 1.5$	2.7	$\widehat{D} = 1.0$
$1.5 < D \leqslant 2.5$	0.6	$\widehat{D} = 2.0$
$D \geqslant 2.5$	0.2	$\widehat{D} = 3.0$

4. Results

4.1. Estimates of coverage range

In addition to the assumptions made on the transmitter in Section 1, we assume on the receiver side, a 0 dB antenna gain and minimum received power requirements of −93 dBm for an IEEE 802.11b 1 Mbps link and −84 dBm for an IEEE 802.11 b 11 Mbps link. These are typical received power requirements cited by manufacturers [17]. Visualization of the antenna coverage patterns will be defined by these two minimum power requirements.

Given the above assumptions and minimum power requirements, we first estimate the coverage range by computing the link budget [18]. The received carrier power, C (in Watts) can be computed as

$$C = \mathrm{EIRP} \times G_R / L_S, \quad (1)$$

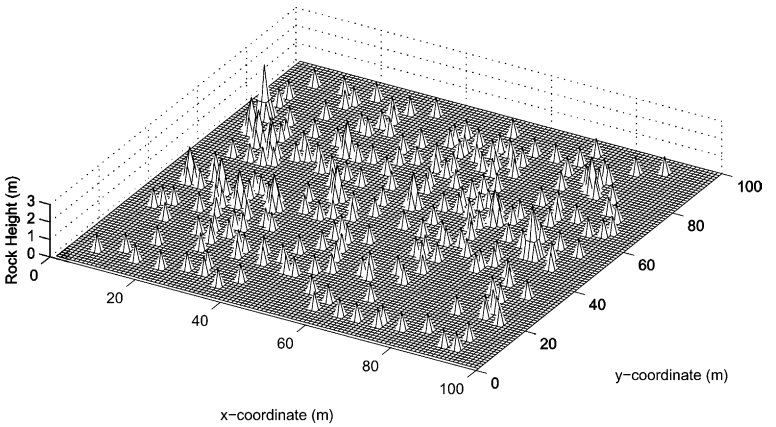

Fig. 2. Sample synthetic clutter layer illustrating location and sizes of rocks.

where EIRP is the effective isotropic radiated power, G_R is the gain of the receiving antenna, and L_S is the space loss. The space loss is defined as

$$L_S \equiv (4\pi R/\lambda)^{2n}, \tag{2}$$

where R is the link range and n is the propagation factor. By substituting (2) into (1) and solving for R, we have a free-space ($n = 1$) range of 5 km for the minimum received power level of -84 dBm and a range of 14 km for the minimum received power level of -93 dBm. These estimated distances are based on free-space propagation without considering terrain effects. On flat terrain, ground-level multipath propagation may be present. Also, when transmitting to or from an antenna located on a hill, scattering and diffraction effects may be present from nearby terrain features. Both of these effects may affect the link propagation distance.

4.2. Coverage metrics

In addition to the actual RF coverage patterns, we also quantify the coverage with the following metrics. The first metric we define is the *Site Coverage* (SC),

$$\mathrm{SC} \equiv \frac{A_{-84}}{A_{\mathrm{CR}}}, \tag{3}$$

where A_{-84} is the area (in m^2) where RF power is -84 dBm or greater and A_{CR} is the area (in m^2) of the Coverage Region (CR). For all sites, the CR is a 2 km × 2 km rhombus which fits inside the map "strips" of Fig. 1. For the selected sites, the A_{CR} is approximately 3.966 km^2.

The second metric we define is the *maximum coverage distance* in the CR or d_{max},

$$d_{\max} \equiv \max[d(x_{\mathrm{TX}}, x_{-84})], \tag{4}$$

where $d(x, y)$ is defined as the distance (in m) from point x to point y, x_{TX} is the location of the transmitter, and x_{-84} is the location of the center of any 66 m × 66 m area where RF power is -84 dBm or greater. This metric is illustrated in Fig. 3. The 66 m × 66 m or 6 pixel × 6 pixel square (at 11 m/pixel) represents 0.1% × A_{CR}. This distance measure prevents tiny areas of measurable RF power

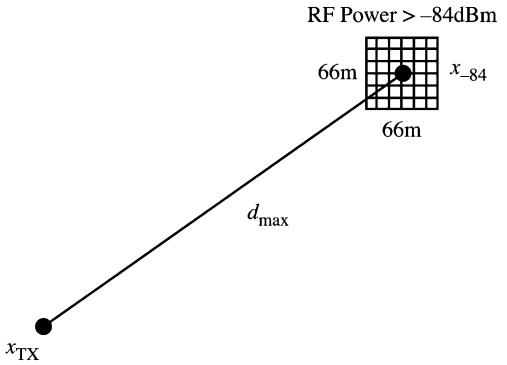

Fig. 3. Illustration of the d_{max} metric defined in (4).

in the simulation from yielding a wireless network range which is larger than can be practically used.

4.3. RF coverage patterns

Figs. 4–8 illustrate the RF coverage patterns for the selected sites of Table 3. The areas in red denote a received power between −85 dBm and −93 dBm and can (in theory) support a 1 Mbps IEEE 802.11b link; the areas in green denote a received power greater than −84 dBm and can (in theory) support an 11 Mbps IEEE 802.11b link. Table 5 provides the SC and d_{max} metrics for each simulation as described above. We note that for the Gusev3, the coverage region is a 1.5 km × 2 km parallelogram centered on the transmitter as opposed to the 2 km × 2 km rhombus for the other sites. This change was due to the fact that the strip maps for Gusev3 are only 1.5 km wide. These figures and associated data demonstrate the potential site coverage in areas of interest on Mars and the possibility of wireless links in excess of 1 km using a 1 W, 2.4 GHz network access point similar in nature to a standard WiFi component. Furthermore, these results illustrate how such RF propagation software can aid in the design of future proximity

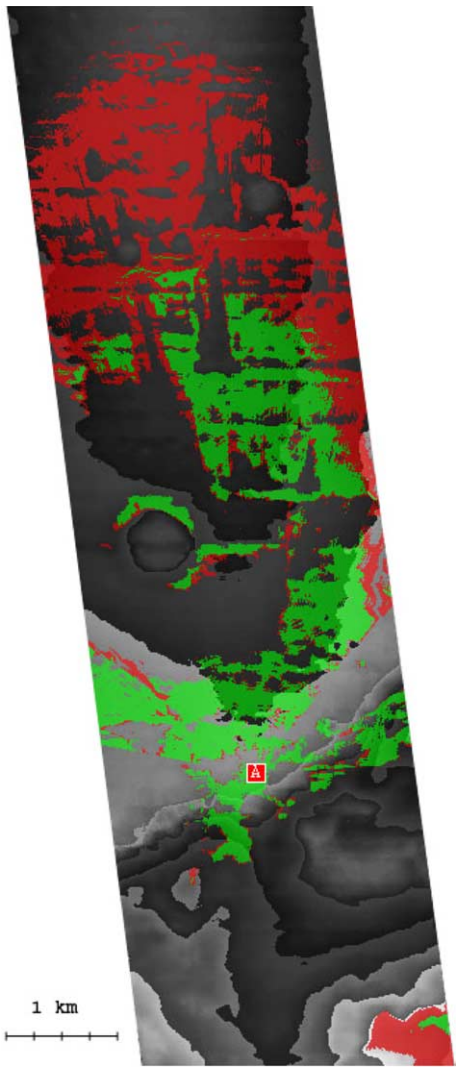

Fig. 4. Antenna coverage pattern for Gusev1, Site 1 (see Fig. 1). Red square with "A" indicates location of transmitter. Red areas denote 1 Mbps, green areas denote 11 Mbps. (For interpretation of the references in colour in this figure legend, the reader is referred to the web version of this article.)

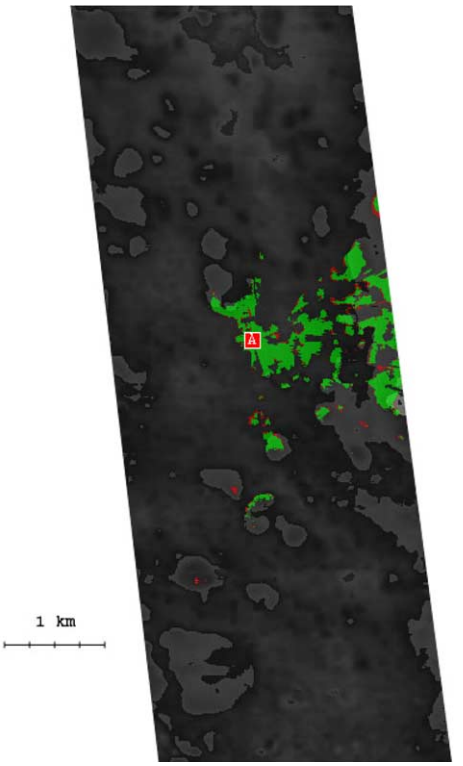

Fig. 5. Antenna coverage pattern for Gusev1, Site 2 (see Fig. 1). Red square with "A" indicates location of transmitter. Red areas denote 1 Mbps, green areas denote 11 Mbps. (For interpretation of the references in colour in this figure legend, the reader is referred to the web version of this article.)

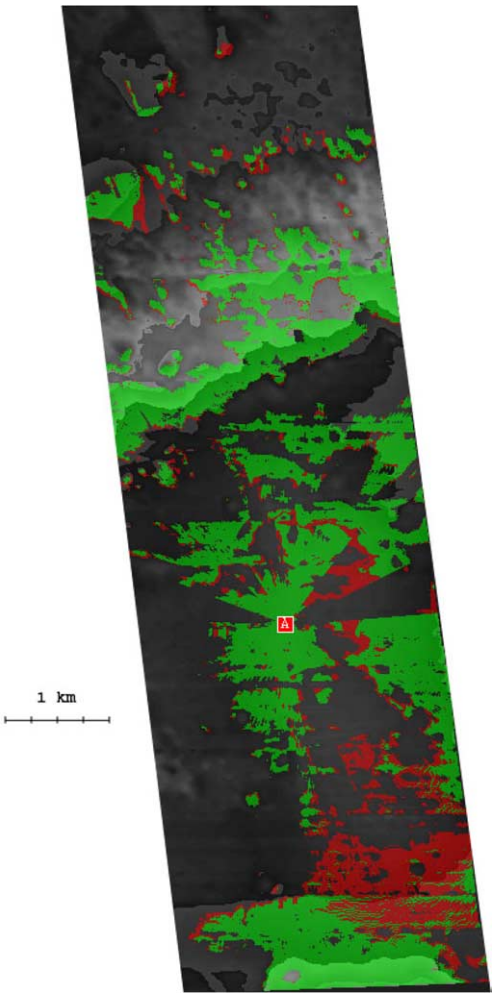

Fig. 6. Antenna coverage pattern for Gusev1, Site 3 (see Fig. 1). Red square with "A" indicates location of transmitter. Red areas denote 1 Mbps, green areas denote 11 Mbps. (For interpretation of the references in colour in this figure legend, the reader is referred to the web version of this article.)

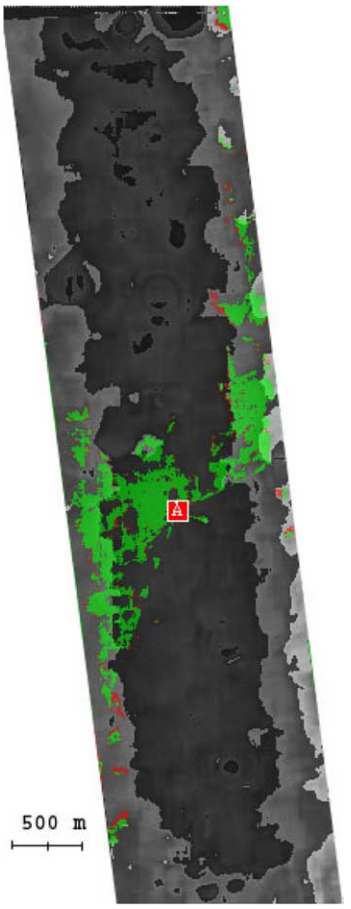

Fig. 7. Antenna coverage pattern for Gusev3, Site 1 (see Fig. 1). Red square with "A" indicates location of transmitter. Red areas denote 1 Mbps, green areas denote 11 Mbps. (For interpretation of the references in colour in this figure legend, the reader is referred to the web version of this article.)

wireless networks or in planning travel routes of rovers after deployment.

In Table 5, we notice that the simulated link range for Gusev3, Site 1, appears to exceed the estimated 5 km distance given earlier. A free-space LOS analysis shows that the performance is 2 dB better than expected. This link is illustrated in Fig. 9 and shows that the path is free of obstructions. However, there are numerous hills just outside the first Fresnel zone of the LOS path that could scatter energy into the field of view of an omnidirectional antenna at the receiver location. These types of complicated paths are not taken into the estimate and would require more detailed analysis.

4.4. Impact of rock clutter on RF coverage

Assuming an antenna height of 1 m, any surface clutter such as rocks of similar height will naturally impact RF coverage. Using the combined synthetic clutter layer with the Gusev1, Site 1 DEM (2 km × 2 km at 1 m/pixel resolution), we can simulate RF coverage patterns and acquire

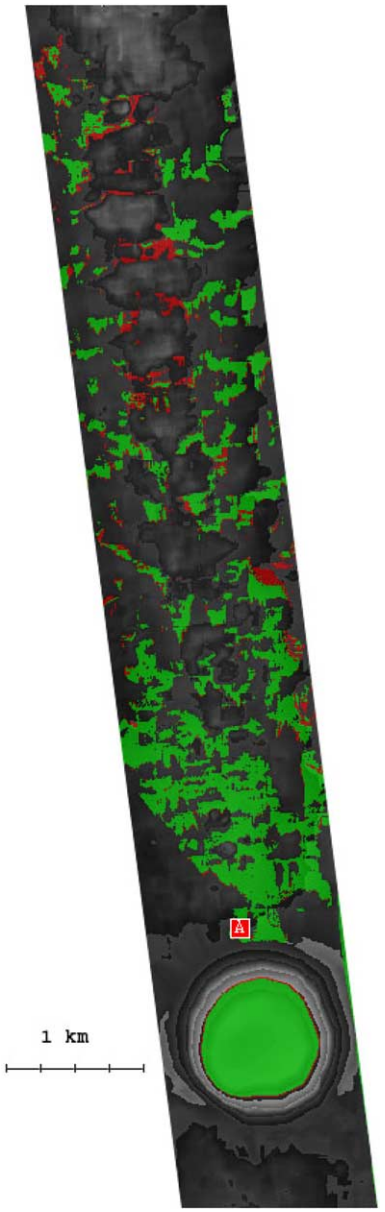

Fig. 8. Antenna coverage pattern for Gusev3, Site 2 (see Fig. 1). The red square with "A" indicates location of transmitter. Red areas denote 1 Mbps, green areas denote 11 Mbps. (For interpretation of the references in colour in this figure legend, the reader is referred to the web version of this article.)

statistics as above. The RF coverage pattern in the presence of clutter is shown in Fig. 10 and resulting metrics are given in Table 6. Because the clutter was synthesized according to statistics at *other*

Table 5
Metrics for RF coverage sufficient for an 11 Mbps IEEE 802.11b link

Site	Site coverage (%)	Maximum coverage distance, d_{max} (m)
Gusev1, Site 1	29.45	3857.8
Gusev1, Site 2	22.78	1888.5
Gusev1, Site 3	26.16	4621.0
Gusev3, Site 1	33.49	6240.3
Gusev3, Site 2	30.45	1632.2

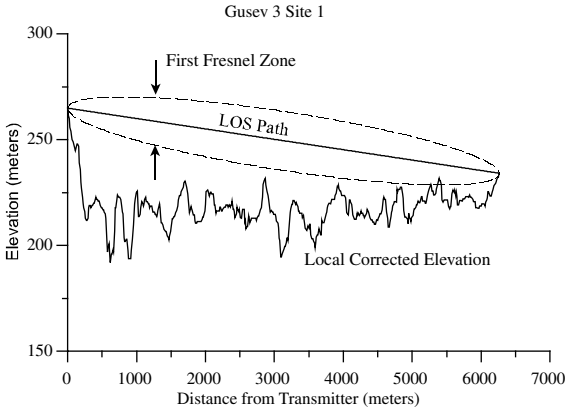

Fig. 9. Terrain profile of Gusev3, Site1, illustrating longer link range due to elevated antennas.

sites and rock sizes were *quantized* to the nearest meter, the resulting metrics for this simulation are only an estimate. The maximum coverage distance for Gusev1, Site 1 without clutter in Table 6 differs from that in Table 5 because the latter is based on the 11 m/pixel, 2 km × 10 km DEM of Fig. 1. This DEM provides a larger area over which to search for remote areas of significant RF power. For the same reason, Gusev1, Site 1 site coverage values in Tables 5 and 6 differ. These clutter results do, however, illustrate the potential for quickly adding in situ knowledge to a lower-resolution DEM to improve predictions of RF coverage for a specific area.

5. Mission planning applications

With the capability to simulate RF coverage patterns, based on actual Martian topography

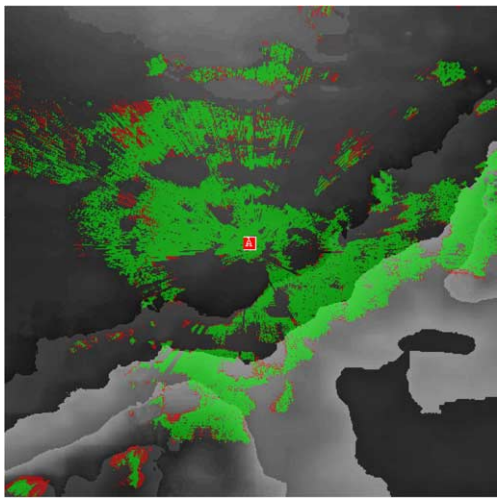

Fig. 10. Antenna coverage pattern for Gusev1, Site 1 (see Fig. 1) with synthetic clutter layer. Red square with "A" indicates location of transmitter. Red areas denote 1 Mbps, green areas denote 11 Mbps. (For interpretation of the references in colour in this figure legend, the reader is referred to the web version of this article.)

Table 6
Metrics for RF coverage sufficient for an 11 Mbps IEEE 802.11b link at selected sites

Site	Site coverage (%)	Maximum coverage distance, d_{max} (m)
Gusev1, Site 1 (without clutter)	32.42	1337.8
Gusev1, Site 1 (with clutter)	19.55[a]	1185.3[a]

[a] Estimate.

and propagation characteristics, mission planners can consider various scenarios or answer questions regarding wireless networking of sensors or rovers. For example, assuming a network access point with an omnidirectional antenna (1 m height) and 1 W radiated power, one might ask: "given the location of a network access point, what is the largest circular area with complete RF coverage?" or "for a given radius from a network access point, what percentage of the area has RF coverage?" or, "given a rover's travel vector, what is the percentage of RF coverage in route."

As a simple example toward answering the first two questions, we consider Gusev1, Sites 1 and 3 as the locations of a network access point [see Fig. 1(a)]. We can acquire data regarding the percentage of RF coverage as a function of distance from the network access point directly from the coverage patterns in Figs. 4 and 6. This data is illustrated in Fig. 11. From the graphs, we can see that for Gusev1, Site1, the largest circular area (with the network access point at the center) capable of supporting either a 1 or 11 Mbps link has a radius of 33 m. For Gusev1, Site3, the largest circular area (with the network access point at the center) capable of supporting either a 1 or 11 Mbps

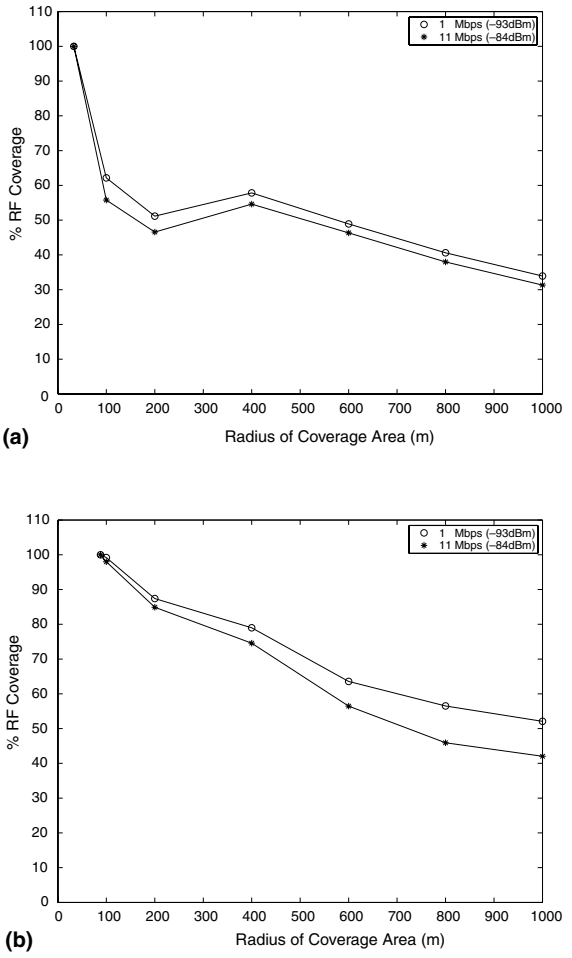

Fig. 11. RF coverage as a function of distance from network access point: (a) Gusev1, Site 1 and (b) Gusev1, Site 3. Areas capable of supporting 1, 11 Mbps in an IEEE 802.11 b link require at least −93 dBm, −84 dBm, respectively.

link has a radius of 88 m. Also from the graph we can see that for a radius of 1000 m, 52%, 42% of the coverage area is capable of supporting a 1, 11 Mbps link, respectively.

6. Conclusions

In this paper, we have contributed to development of a more accurate RF channel model for use in evaluating the performance of wireless proximity networks on the surface of Mars. The work focusses on simulating RF coverage patterns for selected sites on Mars taking into account the local topography and other variables. In addition, clutter models were also developed based on rock statistics on Mars, and their impact on coverage was also quantified. Our work suggests that in the absence of large rocks, sufficient site coverage and long links could be established on the surface of Mars, using elements typical of current wireless networks such as IEEE 802.11b. Such a network could simplify the integration of rovers and sensors used in the exploration of Mars.

Acknowledgement

The authors wish to acknowledge support for this research under NASA Grant NAG3-2864.

References

[1] NASA Space Communications Project. Available from: <http://scp.grc.nasa.gov/portfolio/pn/index.html> (March 2004).
[2] J. Andersen, T. Rappaport, S. Yoshida, Propagation measurements and models for wireless communications channels, IEEE Commun. Mag. 33 (1995) 42–49.
[3] D. Hansen, M. Sue, T. Peng, F. Manshadi, Frequencies for Mars local high-rate links, The Interplanetary Network Progress Report, vol. 42–153, May 2003.
[4] A. Mishkin, J. Morrison, T. Nguyen, H. Stone, B. Cooper, B. Wilcox, Experiences with operations and autonomy of the Mars pathfinder microrover, in: Proceedings of IEEE Aerospace Conference, 1998.
[5] D. Hansen, M. Sue, C. Ho, M. Connally, T. Peng, R. Cesarone, W. Horne, Frequency bands for Mars in situ communications, in: Proceedings of IEEE Aerospace Conference, 2001.
[6] ATDI. Available from: <http://www.atdi.com>.
[7] G. Hufford, A. Longley, W. Kissick, A guide to the use of the ITS irregular terrain model in the area prediction mode, NTIA Report No. 82-100 NTIS Order No. PB82-217977.
[8] S. Cummer, W. Farrell, Radio atmospheric propagation on Mars and potential remote sensing applications, J. Geophys. Res. 104 (1999) 14149–14157.
[9] D. Smith, M. Zuber, The relationship between MOLA northern hemisphere topography and the 6.1 mbar atmospheric pressure surface of Mars, Geophys. Res. Lett. 25 (24) (1998) 4397–4400.
[10] C. Ho, S. Slobin, M. Sue, E. Njoku, Mars background noise temperatures received by spacecraft antennas, The Interplanetary Network Progress Report, vol. 42–149, May 2002.
[11] P. McKenna, Private communication, July 2003.
[12] D. Smith, G. Neumann, R. Arvidson, E. Guinness, S. Slavney, Mars global surveyor laser altimeter mission experiment gridded data record, NASA Planetary Data System (MGS-M-MOLA-MEGDR-L3-V1.0), 2003.
[13] R. Kirk, L. Soderblom, E. Howington-Kraus, B. Archinal, USGS high-resolution topomapping of Mars with Mars orbiter camera narrow-angle images, in: Int. Arch. Photogramm. Remote Sens, Part 4: GeoSpatial Theory, Processing and Applications, vol. 34, 2002.
[14] F. Anderson, A. Haldemann, N. Bridges, M. Golombek, T. Parker, Analysis of MOLA data for the Mars Exploration Rover landing sites, J. Geophys. Res. 108 (E12) (2003), doi:10.1029/2003JE002125.
[15] R. Kirk, E. Howington-Kraus, B. Redding, D. Galuszka, T. Hare, B. Archinal, L. Soderblom, J. Barrett, High-resolution topomapping of candidate MER landing sites with Mars Orbiter Camera narrow-angle images, J. Geophys. Res. 108 (E12) (2003), doi:10.1029/2003JE002131.
[16] M. Golombek, H. Moore, A. Haldemann, T. Parker, J. Schofield, Assessment of Mars pathfinder landing site predictions, J. Geophys. Res. 104 (1999) 8585–8594.
[17] Aztech Technical Specifications for WL500PC Wireless LAN IEEE802.11b PC Card. Available from: <http://www.aztech.com/spec/spec_wl500pc.htm> (March 2004).
[18] S. Horan, Introduction to PCM Telemetering Systems, second ed., CRC Press, Boca Raton, FL, 2002.

Vishwanath Chukkala received the B.Tech. Electronics and Communications Engineering from the Jawaharlal Nehru Technological University, India in 2001 and the M.S. degree in Electrical Engineering from New Mexico State University in 2003. His research interests are in wireless communications and real time DSP.

Phillip DeLeon received the B.S. Electrical Engineering and the B.A. in Mathematics from the University of Texas at Austin, in 1989 and 1990 respectively and the M.S. and Ph.D. degrees in Electrical Engineering from the University of Colorado at Boulder, in 1992 and 1995 respectively. Previously he worked at AT&T (and later Lucent Technologies) Bell Laboratories in Murray Hill, N.J. Currently, he serves as an Associate Professor in the Klipsch School, Director of the Advanced Speech and Audio Processing Laboratory, and Associate Director of the Center for Space Telemetering and Telecommunications at NMSU. His research interests are in adaptive-, multirate-, real-time-, and speech-signal processing as well as wireless communications. Dr. De Leon is a senior member of IEEE.

Stephen Horan received the A.B. degree in physics from Franklin and Marshall College, Lancaster, PA, the M.S. degree in astronomy, the M.S.E.E. degree, and the Ph.D. degree in electrical engineering, all from New Mexico State University, Las Cruces, in 1979, 1981, and 1984, respectively. From 1984 through 1986, he was a software engineer and systems engineer with Space Communications Company at the NASA White Sands Ground Terminal where he was involved with the software maintenance and specification for satellite command and telemetry systems and operator interfaces. In 1986, he joined the faculty at New Mexico State University, where he is presently a Professor and holder of the Frank Carden Chair of the Telemetering and Telecommunications Program, Klipsch School of Electrical and Computer Engineering. His research and teaching interests are in space communications and telemetry systems. He is the author of Introduction to PCM Telemetering Systems (Boca Raton, FL: CRC). Dr. Horan is a senior member of AIAA and IEEE and a member of Eta Kappa Nu.

Vijayakumar Velusamy received the B.E. degree in Electronics and Communication Engineering from Bharathiar University, India in 2001 and the M.S. in Electrical Engineering from New Mexico State University in 2003. His research interests are wireless communications, coding theory and data communication networks.